Kinetic energy density functionals from the Airy gas with an application to the atomization kinetic energies of molecules

Lucian A. Constantin and Adrienn Ruzsinszky
Department of Physics and Quantum Theory Group, Tulane University, New Orleans, Louisiana 70118, USA
(Received 1 December 2008; revised manuscript received 22 January 2009; published 19 March 2009)

We construct and study several semilocal density-functional approximations for the positive Kohn-Sham kinetic energy density. These functionals fit the kinetic energy density of the Airy gas and they can be accurate for integrated kinetic energies of atoms, molecules, jellium clusters, and jellium surfaces. We find that these functionals are the most accurate ones for atomization kinetic energies of molecules and for fragmentation of jellium clusters. We also report that local and semilocal kinetic energy functionals can show "binding" when the density of a spin-unrestricted Kohn-Sham calculation is used.

DOI: 10.1103/PhysRevB.79.115117 PACS number(s): 71.15.Mb, 31.15.E−, 71.45.Gm

I. INTRODUCTION

The positive Kohn-Sham (KS) (Ref. 1) kinetic energy (KE) density of noninteracting electrons,

$$\tau(\mathbf{r}) = \frac{1}{2}\sum_{i}^{N} |\nabla \phi_i(\mathbf{r})|^2, \tag{1}$$

is an exact functional of the occupied orbitals $\{\phi_i\}$. Density-functional approximations to the noninteracting kinetic energy $T_s[n_\uparrow, n_\downarrow] = \int d\mathbf{r}\, \tau(\mathbf{r})$ can simplify and speed up by orders of magnitude any KS self-consistent calculation.[2] [Here $n_\uparrow(\mathbf{r})$ and $n_\downarrow(\mathbf{r})$ are the spin densities.] However, in spite of important and hard work done in this direction,[3] no actual approximation has reached chemical accuracy.

The simplest model of an edge electron gas is the Airy gas, where any electron feels a linear effective potential,[4] and thus the normalized one-particle eigenfunctions are proportional to the Airy function. The effective finite-linear-potential model gives remarkably good results for the jellium surface problem.[5,6] However, the KE density derived in this approximation[7] does not recover the correct second-order gradient expansion KE density[8,9] and has an unphysical oscillating behavior in the limit of slow density variations,[10] being a poor approximation for atoms.[11]

The positive KE density of the Airy gas was studied by Vitos, Johansson, Kollár, and Skriver,[12] and they derived a generalized gradient approximation (GGA) density functional for $\tau(\mathbf{r})$. (This approximation is denoted in this paper by VJKS GGA.) They showed that the poor behavior of the kinetic energy density derived in the linearized-potential approximation[7] is mainly due to a Laplacian term that arises naturally in the Airy gas model. Thus, the Laplacian term, even if it integrates to zero and does not affect the integrated KE, is an important tool in developing density functionals not only for the KE but also for the exchange-correlation (xc) energy.[12,13] The VJKS GGA KE density functional fits the Airy gas KE density and is a good model for the KE density of the jellium surfaces, but for atoms and molecules it diverges to $-\infty$ at the nuclei due to the behavior of the Laplacian term. The integrated kinetic energies are at a Thomas-Fermi[14] level of accuracy, reducing considerably the error of the linearized-potential approximation.[7]

A jellium surface is the simplest model of a metallic surface. Self-consistent local-spin-density (LSD) calculations[15] for this model provided early evidence that density functionals may work. But wave function-based methods, such as Fermi hypernetted chain[16] and diffusion Monte Carlo (DMC) of Ref. 17, predicted low-density surface xc energies about 40% larger than those from LSD. Recent refined DMC estimates,[18] and calculations in the random phase approximation[19,20] and beyond it,[21–23] agree with the popular xc semilocal density functionals, showing that the jellium surface cannot only be accurately described in the context of density-functional theory, but can also be an important model used to develop new density functionals.

The exchange energy density of the Airy gas[4,24,25] and the xc jellium surface energies[25,26] were employed in the construction of accurate xc GGA's for solids (see Refs. 24–26). A simple xc GGA functional depends only on spin densities and their gradients and cannot describe accurately both solids and atoms.[27] However, a Laplacian-level xc meta-GGA,[13] which depends nontrivially on spin densities and their gradients and Laplacians, can be accurate for atoms, molecules, solids, and surfaces.

In this paper, we derive several GGA KE functionals from the Airy gas and jellium surfaces and we find them accurate for atomization KE energies of molecules and for fragmentation of jellium clusters. Our functionals, constructed similarly to that of Ref. 12, recover the second-order gradient expansion of the integrated KE, have the right behavior of the KE density in the tail of the density, and fit the kinetic energy density of the Airy gas.

The paper is organized as follows. In Sec. II, we construct our KE functionals. In Sec. III we test the functionals for atoms, jellium clusters, jellium surfaces, and molecules. In Sec. IV, we summarize our conclusions.

II. LAPLACIAN-DEPENDENT GGA KINETIC ENERGY FUNCTIONALS

The positive kinetic energy density of the local Airy gas (LAG) is[12]

$$\tau^{\mathrm{LAG}}(z) = -\frac{3}{5}n(z)v_{\mathrm{eff}}(z) + \frac{1}{5}\nabla^2 n(z), \tag{2}$$

where $v_{\mathrm{eff}}(z)$ is the effective potential and $n(z)$ is the density of the Airy gas. (Unless otherwise stated, atomic units are

used throughout, i.e., $e^2=\hbar=m_e=1$.) Alternatively, Eq. (2) can be written[12] using the Thomas-Fermi kinetic energy density $\tau^{\mathrm{TF}}=(3/10)(3\pi^2)^{2/3}n^{5/3}$:

$$\tau^{\mathrm{LAG}}(z)=\tau^{\mathrm{TF}}(z)P(z)+\frac{1}{5}\nabla^2 n(z), \tag{3}$$

where

$$P(z)=-\frac{2Bz}{(3\pi^2)^{2/3}n(z)^{2/3}}, \tag{4}$$

and B is the slope of the linear effective potential. $P(z)$ is a smooth function of the reduced density gradient,

$$s(\mathbf{r})=|\nabla n(\mathbf{r})|/[2k_F(\mathbf{r})n(\mathbf{r})], \tag{5}$$

where $k_F(\mathbf{r})=[3\pi^2 n(\mathbf{r})]^{1/3}$ is the Fermi wave vector. (The dimensionless density gradient $s(\mathbf{r})$ measures the variation of the density over a Fermi wavelength $\lambda_F=2\pi/k_F$.) Thus, Vitos *et al.*[12] proposed the following GGA KE density functional

$$\tau^{\mathrm{VJKS}}(\mathbf{r})=\tau^{\mathrm{TF}}(\mathbf{r})P^{\mathrm{VJKS}}(s(\mathbf{r}))+\frac{1}{5}\nabla^2 n(\mathbf{r}), \tag{6}$$

where

$$P^{\mathrm{VJKS}}(s)=\frac{1+0.8944s^2-0.0431s^6}{1+0.6511s^2+0.0431s^4} \tag{7}$$

fits $P(z)$ for the Airy gas model. Equation (6) recovers the exact KE density of the von Weizsäcker functional[28] $|\nabla n|^2/(8n)=(5/3)\tau^{\mathrm{TF}}s^2$ for an exponentially decaying density (see Ref. 29), but for a slowly varying density behaves as $\tau^{\mathrm{TF}}[1+0.2433s^2+O(s^4)]+\frac{1}{5}\nabla^2 n(z)$ and violates the second-order gradient expansion (GE2) of the KE density[8,9]

$$\tau^{\mathrm{GE2}}=\tau^{\mathrm{TF}}\left(1+\frac{5}{27}s^2\right)+\frac{1}{6}\nabla^2 n. \tag{8}$$

Let us consider the following arbitrary partition of Eq. (3) for the Airy gas model:

$$\tau^{\mathrm{LAG}}(z)=\tau^{\mathrm{TF}}(z)F(z,\beta)+\beta\nabla^2 n. \tag{9}$$

Equations (3) and (9) give

$$F(z,\beta)=P(z)+\frac{[(1/5)-\beta]\nabla^2 n(z)}{\tau^{\mathrm{TF}}(z)}. \tag{10}$$

$F(z,\beta)$ is a smooth function of the reduced gradient s for any $\beta>1/8$, and it can be accurately approximated by the following expression:

$$F^{\mathrm{CR}}(s,\beta)=\frac{1+(a_1+5/27)s^2+a_2s^4+a_3s^6-a_4s^8}{1+a_1s^2+a_5s^4+\frac{3}{40\beta-5}a_4s^6}, \tag{11}$$

where a_1, a_2, a_3, a_4, and a_5 are parameters that depend on β. Equation (11) recovers the terms $1+(5/27)s^2$ for a slowly varying density, but the second-order gradient expansion of the KE density additionally requires that $\beta=1/6$. In the tail, where the density decays exponentially, Eqs. (9) and (11) give the correct KE density of the von Weizsäcker functional.

TABLE I. Parameters of the enhancement factor $F^{\mathrm{CR}}(s,\beta)$ for various GGAs.

	$A\frac{1}{5}$-GGA	$A\frac{1}{6}$-GGA	$A0.185$-GGA
a_1	1.122609	1.301786	1.293576
a_2	0.900085	3.715282	2.161116
a_3	−0.227373	0.343244	−0.144896
a_4	0.014177	0.032663	0.025505
a_5	0.731298	2.393929	1.444659

When $\beta=1/5$, $F(z,\beta=1/5)=P(z)$ and we define a GGA ($A\frac{1}{5}$) similar with the one in Ref. 12,

$$\tau^{A(1/5)}(\mathbf{r})=\tau^{\mathrm{TF}}(\mathbf{r})F^{\mathrm{CR}}[s(\mathbf{r}),\beta=1/5]+\frac{1}{5}\nabla^2 n(\mathbf{r}), \tag{12}$$

where the fitting parameters are shown in Table I.

When $\beta=1/6$, we define a GGA ($A\frac{1}{6}$) that recovers the second-order gradient expansion KE density,

$$\tau^{A(1/6)}(\mathbf{r})=\tau^{\mathrm{TF}}(\mathbf{r})F^{\mathrm{CR}}[s(\mathbf{r}),\beta=1/6]+\frac{1}{6}\nabla^2 n(\mathbf{r}), \tag{13}$$

where the fitting parameters are shown in Table I.

The Airy gas is the simplest edge electron gas and does not include curvature corrections that are present at the edge surfaces (see Fig. 2 of Ref. 4). Thus in order to find an optimum value of β for jellium surfaces, let us define the quality factor (similarly to Refs. 12 and 30),

$$\delta(\beta)=\int d\mathbf{r}|\tau^{\mathrm{approx}}(\mathbf{r},\beta)-\tau(\mathbf{r})|/\int d\mathbf{r}\,\tau(\mathbf{r}), \tag{14}$$

where τ^{approx} is an approximation of the positive Kohn-Sham KE density τ. [See Eq. (1)]. We apply the quality factor to jellium surfaces using numerical LSD Kohn-Sham orbitals and densities.[15,31] The integration was done from $z_{\min}=-2.75\lambda_F$ to $z_{\max}=2\lambda_F$, where $\lambda_F=2\pi/k_F$ is the bulk Fermi wavelength, for several values of bulk parameter r_s. [Here $r_s=(9\pi/4)^{1/3}/k_F$ is the radius of a sphere which contains on average one electron, and k_F is the bulk Fermi wave vector.] For τ^{approx} we use Eqs. (9) and (11). Thus, for values of β between 0.15 and 0.22, we accurately fit $F(z,\beta)$ with the Padé approximation of Eq. (11), and we calculate $\delta(\beta)$. Figure 1 shows that $\delta(\beta)$ is minimum for $\beta\approx 0.185$ for semi-infinite jellium surfaces with $r_s=2$, 3, and 4.

So from our jellium surface analysis we define the following GGA ($A0.185$) that also fits the kinetic energy density of the Airy gas:

$$\tau^{A0.185}(\mathbf{r})=\tau^{\mathrm{TF}}(\mathbf{r})F^{\mathrm{CR}}[s(\mathbf{r}),\beta=0.185]+0.185\nabla^2 n(\mathbf{r}), \tag{15}$$

where the fitting parameters are shown in Table I.

In Fig. 2 we show the exact function $F(z,\beta)$ and the fitting function $F^{\mathrm{CR}}(s,\beta)$ versus the scaled density gradient s, for $\beta=1/5$, 1/6 and 0.185, respectively. Up to $s=3$, the exact functions F and the parameterized ones cannot be distinguished. (We note that s values bigger than 3 are found in the

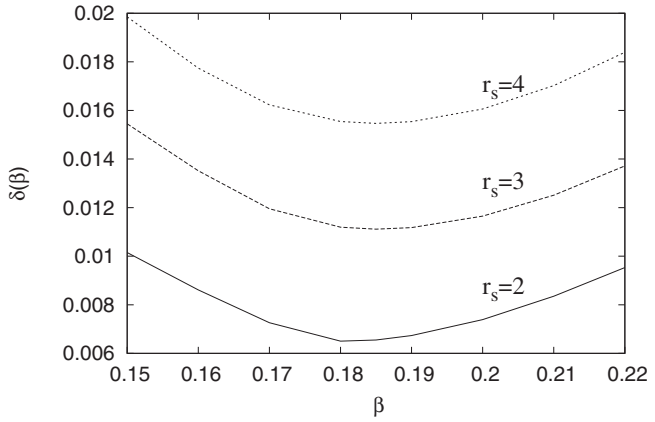

FIG. 1. The quality factor $\delta(\beta)$ versus β, for τ^{approx} given by Eqs. (9) and (11), for the jellium surfaces with bulk parameters $r_s=2$, 3, and 4. We use LSD KS orbitals and densities (Refs. 15 and 31).

tail of an atom or molecule, where the electron density is negligible.) $P^{\text{VJKS}}(s)$ overestimates $P(z)=F(z,\beta=1/5)$ until $s\approx 3$ and underestimates $P(z)$ for $3\leq s\leq 10$.

Far from the edge of the Airy gas, the density has Friedel oscillations.[4] These oscillations are well described by the kinetic energy density of the linear potential approximation[7] that in the slowly varying density regime reduces to[10]

$$\tau^{\text{lin}}=\tau^{\text{TF}}+\frac{5}{72}\frac{(\nabla n)^2}{n}+\frac{1}{12}\frac{(\nabla n)^2}{n}\sin\left(\frac{2(3\pi^2)^{1/3}n^{4/3}}{|\nabla n|}\right). \tag{16}$$

The third term represents quantum oscillations and has an unphysical behavior when $\nabla n\to 0$. In Fig. 3 we show $\tau-\tau^{\text{TF}}$ versus ζ, for a slowly varying Airy gas density. The edge is at $\zeta=0$. [$\zeta=(2B)^{1/3}z$ is the scaled spatial coordinate for the Airy gas.] The Friedel oscillations are well described by Eq. (16). But even if $\tau^{A(1/6)}-\tau^{\text{TF}}$ is the worst kinetic energy density shown in the figure, its integration over a period

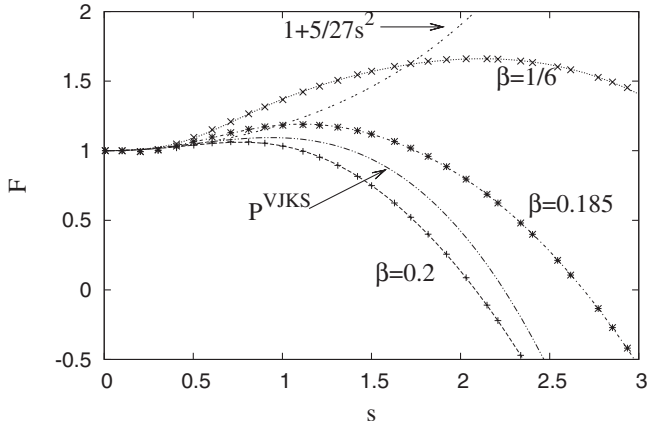

FIG. 2. The exact function $F(z,\beta)$ shown with points $[F(z,\beta),s(z)]$ for some discrete z, and parameterized function $F^{\text{CR}}(s,\beta)$ shown with lines for $\beta=1/5,1/6$, and 0.185, versus the reduced gradient s, for the Airy gas model. Also shown are the enhancement factor $(1+5/27s^2)$ and $P^{\text{VJKS}}(s)$.

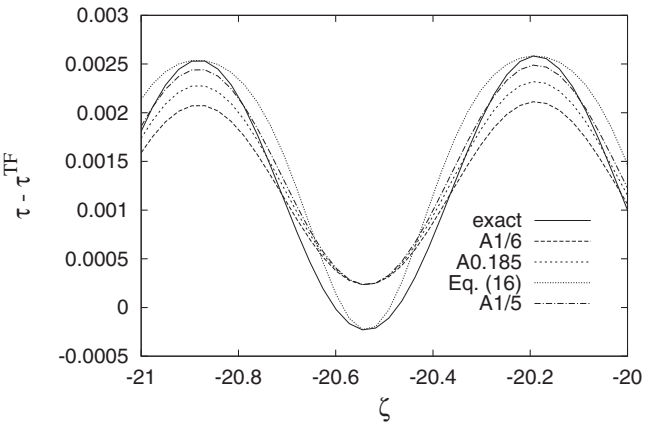

FIG. 3. $\tau-\tau^{\text{TF}}$ versus ζ for the Airy gas model. The edge is at $\zeta=0$. The integrations of $\tau-\tau^{\text{TF}}$ over the complete Friedel oscillation shown in figure are: $T_s^{\text{exact}}-T_s^{\text{TF}}=8.30\times10^{-4}$, $T_s^{A(1/5)}-T_s^{\text{TF}}=9.58\times10^{-4}$, $T_s^{A(1/6)}-T_s^{\text{TF}}=8.26\times10^{-4}$, $T_s^{A0.185}-T_s^{\text{TF}}=8.98\times10^{-4}$, and $T_s^{\text{lin}}-T_s^{\text{TF}}=9.89\times10^{-4}$. VJKS GGA, not shown in the figure, gives an integrated value of 10.09×10^{-4}.

of the Friedel oscillations is almost exact. Thus $\tau^{A(1/6)}$, which behaves as τ^{GE2} in this limit, is the best approximation for the integrated KE, whereas τ^{lin} gives the worst integrated KE.

III. TESTS OF OUR GGA KINETIC ENERGY FUNCTIONALS

In this section we test our functionals for various systems. In the calculations we use the spin-scaling relation,[32]

$$\tau_\sigma([n_\sigma],\mathbf{r})=(1/2)\tau([n=2n_\sigma],\mathbf{r}), \tag{17}$$

where n_σ is the density of the electrons with spin σ. ($\sigma=\uparrow$ or $\downarrow$.)

A. Integrated kinetic energies of atoms, jellium clusters, and jellium surfaces

In Table II we show the accuracy of T_s^{TF}, T_s^{VJKS}, T_s^{GE2}, T_s^{GE4}, $T_s^{A(1/5)}$, $T_s^{A(1/6)}$, and $T_s^{A0.185}$ for atoms, jellium clusters, and jellium surfaces (similarly as Table I of Ref. 13). The error displayed in this table is

$$\text{Error}=\frac{1}{2}\text{“ m.a.r.e.atoms ”}+\frac{1}{4}\text{“ m.a.r.e.clusters ”}+\frac{1}{4}\text{“ m.a.r.e.LDM}(N=8)\text{ ”}, \tag{18}$$

where m.a.r.e. atoms is the mean absolute relative error (m.a.r.e.) of the integrated kinetic energy of 50 atoms and ions (listed in Ref. 13), m.a.r.e. clusters is the m.a.r.e. of $2e^-$, $8e^-$, $18e^-$, $20e^-$, $34e^-$, $40e^-$, $58e^-$, $92e^-$, and $106e^-$ neutral spherical jellium clusters (with bulk parameter $r_s=3.93$ which corresponds to Na), and m.a.r.e. LDM($N=8$) is the m.a.r.e. of the KE of $N=8$ jellium spheres for $r_s=2$, 4, and 6, calculated in the liquid drop model[13] (LDM),

TABLE II. Mean absolute relative error (m.a.r.e.) of kinetic energies of 50 atoms and ions (see Ref. 13), of neutral spherical jellium Na clusters ($2e^-$, $8e^-$, $18e^-$, $20e^-$, $34e^-$, $40e^-$, $58e^-$, $92e^-$, and $106e^-$) and of jellium surfaces (with $r_s=2$, $r_s=4$, and $r_s=6$) incorporated into the liquid drop model for a jellium sphere with $N=8$ electrons [see Eq. (19)]. Also shown is the total error given by Eq. (18).

	m.a.r.e atoms	m.a.r.e clusters	m.a.r.e. LDM($N=8$)	Error [Eq. (18)]
T_s^{TF}	0.0842	0.0439	0.0810	0.0733
T_s^{VJKS}	0.0399	0.0465	0.0754	0.0504
T_s^{GE2}	0.0112	0.0099	0.0330	0.016
T_s^{GE4}	0.0251	0.0176	0.0170	0.0212
$T_s^{A(1/5)}$	0.0626	0.0566	0.0879	0.067
$T_s^{A(1/6)}$	0.0789	0.0154	0.0177	0.048
$T_s^{A0.185}$	0.0083	0.0249	0.0535	0.024

$$T_s^{\mathrm{LDM}} = (3/10)k_F^2 N + \sigma_s N^{2/3} 4\pi r_s^2, \tag{19}$$

where k_F is the bulk Fermi wave vector, and σ_s is the surface KE. The exact LDM value is computed with the exact σ_s (using LSD orbitals). Because the relative errors of surface kinetic energies are much larger than those of the atoms and spherical jellium clusters, we use the LDM approach for calculating the jellium surface KE errors (as in Ref. 13); LDM gives m.a.r.e. comparable to that of atoms and clusters (see Table II). We use analytic Hartree-Fock densities and orbitals[33] for atoms and ions, and numerical Kohn-Sham densities and orbitals for jellium clusters [using the optimized potential method (OPM) (Ref. 34)] and jellium semi-infinite surfaces (using LSD xc potential).

τ^{VJKS}, $\tau^{A(1/5)}$, $\tau^{A(1/6)}$, and $\tau^{A0.185}$ are constructed to model the KE density of the Airy gas, but only $\tau^{A(1/6)}$ recovers the second-order gradient expansion of the KE density. The difference between $\tau^{A(1/5)}$ and τ^{VJKS} is given mainly by the quality of fitting the function $P(z)$ of Eq. (4). (See Fig. 2.) $\tau^{A0.185}$ includes effects of density variations near jellium surfaces because of our optimization of the Laplacian coefficient. In Table II we see that $T_s^{A(1/6)}$ is very accurate (comparable with the fourth-order gradient expansion) for jellium systems and gives an overall error smaller than $T_s^{A(1/5)}$ and T_s^{VJKS}. $T_s^{A0.185}$ is accurate for atoms and gives an overall error comparable with the fourth-order gradient expansion one (see also Table I of Ref. 13).

B. Integrated atomization kinetic energy for a set of molecules

In Table III we present the atomization kinetic energies for the molecules used in Refs. 13 and 35. We observe that $T_s^{A(1/5)}$ keeps the right sign for all the molecules and has practically the same mean absolute error as the Thomas-Fermi functional. In Ref. 35 it was shown that the Thomas-Fermi KE functional gives better atomization kinetic energies than all the other tested semilocal functionals. $T_s^{A0.185}$ is accurate for atoms and molecules, and gives the smallest mean absolute error for the atomization energies presented in Table III. We also show that the semilocal functional of Ref. 38, whose parameters are fitted to atoms, works worse than the Thomas-Fermi functional and all the semilocal functionals derived from the Airy gas.

C. Binding energy of the N_2 molecule

In Fig. 4 we show the binding energy of the N_2 molecule as a function of the distance between the nuclei. We use a spin-unrestricted Hartree-Fock calculation in which the spin

TABLE III. Integrated atomization kinetic energy (KE atoms—KE molecule, in a.u.) for the set of molecules used in Refs. 13 and 35. The kinetic energies were calculated using the PROAIMV code with Kohn-Sham orbitals given by the Gaussian 2000 code [with the uncontracted 6-311+$G(3df,2p)$ basis set, Becke 1988 exchange functional (Ref. 36), and Perdew-Wang correlation functional (Ref. 37)]. The last line shows the mean absolute errors (m.a.e.). Here T_s^{TW} is the the GGA of Ref. 38 with the parameters $k=0.8438$ and $\mu=0.2319$.

	T_s^{exact}	T_s^{TF}	T_s^{VJKS}	T_s^{GE2}	$T_s^{A(1/5)}$	$T_s^{A(1/6)}$	$T_s^{A0.185}$	T_s^{TW}
H_2	−0.150	−0.097	−0.086	−0.114	−0.080	−0.114	−0.096	−0.108
HF	−0.185	−0.305	−0.369	−0.186	−0.422	−0.173	−0.311	−0.226
H_2O	−0.304	−0.308	−0.455	−0.136	−0.531	−0.169	−0.369	−0.209
CH_4	−0.601	−0.737	−0.907	−0.571	−0.972	−0.618	−0.813	−0.649
NH_3	−0.397	−0.231	−0.457	−0.060	−0.525	−0.165	−0.364	−0.155
CO	−0.298	−0.323	−0.580	−0.085	−0.678	−0.181	−0.456	−0.203
F_2	−0.053	0.128	0.013	0.282	−0.050	0.269	0.093	0.223
HCN	−0.340	−0.1835	−0.539	0.079	−0.644	−0.097	−0.399	−0.071
N_2	−0.158	0.344	−0.046	0.565	−0.134	0.321	0.069	0.412
CN	−0.431	−0.215	−0.539	0.005	−0.631	−0.168	−0.424	−0.129
NO	−0.268	0.092	−0.215	0.330	−0.313	0.176	−0.094	0.198
O_2	−0.100	0.106	−0.089	0.335	−0.177	0.286	0.030	0.239
m.a.e.		0.177	0.133	0.311	0.172	0.224	0.116	0.232

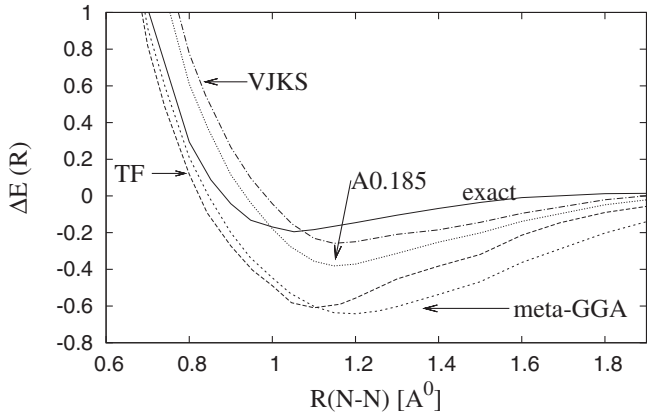

FIG. 4. Binding energy ($\Delta E = E$ molecule—E atoms, in a.u.) as a function of N-N distance for the N_2 molecule using a nonrestricted Hartree-Fock calculation [with uncontracted 6-311+$G(3df,2p)$ basis set]. The curve "meta-GGA" is the binding energy given by the Laplacian-level KE meta-GGA of Ref. 13. The Hartree-Fock density was used as input for orbital-free KE functionals. 1 Å = 1.8897 a.u..

symmetry breaks close to the Hartree-Fock equilibrium bond length. This helps the functionals to show an equilibrium length close to the exact. Figure 4 is in accord with the values for the N_2 molecule listed in Table III; all the semilocal functionals presented in the figure give bigger atomization kinetic energies than the exact calculation, thus showing a minimum in the total energy calculated with the Hartree-Fock density.

The unrestricted solution becomes energetically lower beyond the Coulson-Fisher point[39] than the energy of the restricted solution, and spin-symmetry breaking for the N_2 molecule can be achieved by mixing the highest occupied and lowest unoccupied orbitals.[40] For a spin-restricted calculation, the orbital-free KE functionals listed in Table II do not show an equilibrium point, thus the spin-breaking symmetry[41–43] and the spin-scaling relations[32] play an important role in describing stretched molecules, and they need to be taken into account in the orbital-free codes.

D. Tests of the kinetic energy density

In Fig. 5 we show the kinetic energy density of our functionals at a jellium surface. Though $\tau^{A0.185}$ has the smallest overall error, $\tau^{A(1/6)}$ gives the most accurate surface kinetic energy because it is accurate near the surface and it can almost exactly damp the Friedel oscillations far from the surface (see Fig. 3).

In Fig. 6 we show the kinetic energy densities of our functionals for the $2e^-$ Na jellium cluster. Here the exact curve is the von Weizsäcker[28] KE density. We see that all three functionals ($\tau^{A(1/5)}$, $\tau^{A(1/6)}$, and $\tau^{A0.185}$) recover the exact curve in the tail of the density, as expected.

E. Large-Z asymptotic behavior

The noninteracting kinetic energy of the neutral atoms has the following asymptotic expansion:[44,45]

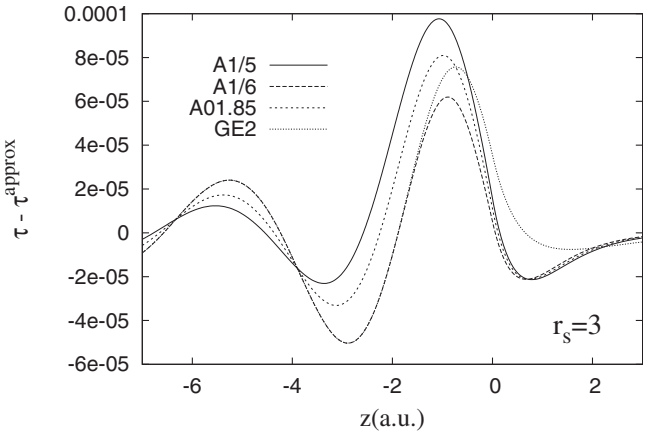

FIG. 5. $\tau(z)-\tau^{\text{approx}}(z)$, where τ^{approx} is $\tau^{A(1/5)}$, $\tau^{A(1/6)}$, $\tau^{A0.185}$, and τ^{GE2}, respectively, versus z, for a jellium surface of bulk parameter $r_s=3$. The surface is at $z=0$, the jellium is at $z\leq 0$ and the vacuum is at $z>0$. The surface kinetic energies are: $\sigma_s^{\text{exact}}=-703$ erg/cm^2, $\sigma_s^{A(1/5)}=-869$ erg/cm^2, $\sigma_s^{A(1/6)}=-690$ erg/cm^2, $\sigma_s^{A0.185}=-788$ erg/cm^2, and $\sigma_s^{GE2}=-762$ erg/cm^2. VJKS GGA, not plotted in the figure, gives $\sigma_s^{\text{VJKS}}=-837$ erg/cm^2. (1 hartree/bohr^2 = 1.557×10^6 erg/cm^2) We use LSD KS orbitals and densities (Refs. 15 and 31).

$$T_s = c_0 Z^{7/3} + c_1 Z^2 + c_2 Z^{5/3}, \tag{20}$$

where Z is the atomic number, and $c_0=0.768745$, $c_1=-1/2$, and $c_2=0.2699$. In Ref. 45 the authors propose an accurate method to extract these coefficients for any KE functional. In Table IV we present the large-Z asymptotic behavior of our functionals. All the functionals listed in Table IV are exact for systems with uniform density, such that we expect that they have the exact Thomas-Fermi coefficient $c_0=0.768745$. (Similarly with Ref. 45, we do not have enough data points to extract c_0 accurately.) $T_s^{A0.185}$ and T_s^{VJKS}, the functionals that give the most accurate atomization kinetic energies, have reasonable large-Z asymptotic behaviors.

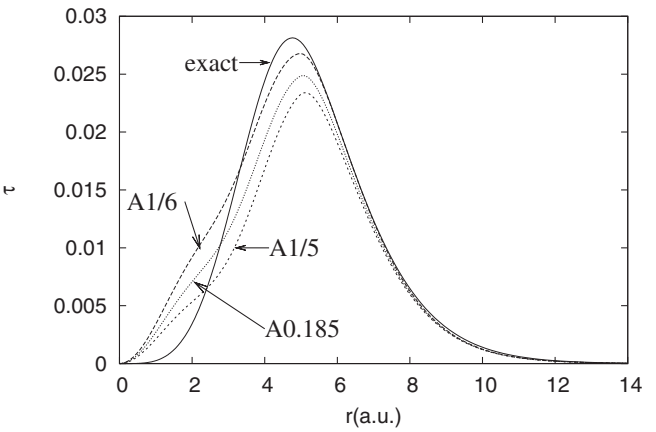

FIG. 6. Kinetic energy density versus radial distance r, for the $2e^-$ jellium cluster (with bulk parameter $r_s=3.93$). The area under the curve is the kinetic energy: $T_s^{\text{exact}}=0.114$ a.u., $T_s^{A(1/5)}=0.098$ a.u., $T_s^{A(1/6)}=0.121$ a.u., and $T_s^{A0.185}=0.108$ a.u. VJKS GGA, not shown in the figure, gives $T_s^{\text{VJKS}}=0.101$ a.u.

TABLE IV. The coefficients of the asymptotic expansion of Eq. (20) for several semilocal functionals. The fitting method is the same as in Ref. 45. We use OPM (Ref. 34) densities.

	c_0	c_1	c_2
Exact	0.768745	−0.500000	0.269900
T_s^{GE2}	0.768745	−0.536197	0.335992
T_s^{TW}	0.768745	−0.507979	0.291815
$T_s^{A(1/5)}$	0.768745	−0.532065	0.229370
$T_s^{A(1/6)}$	0.768745	−0.439745	0.392152
$T_s^{A0.185}$	0.768745	−0.491080	0.302999
T_s^{VJKS}	0.768745	−0.507589	0.225358

F. Fragmentation of jellium clusters

Let us consider the disintegration of the $106e^-$ neutral spherical jellium Na cluster into smaller closed-shell jellium spheres,

$$(106e^-) \rightarrow n_1(92e^-) + n_2(58e^-) + n_3(40e^-) + n_4(34e^-) + n_5(20e^-) + n_6(18e^-) + n_7(8e^-) + n_8(2e^-), \tag{21}$$

where $n_1, \ldots, n_8$ are positive integers, and $92n_1+58n_2+40n_3+34n_4+20n_5+18n_6+8n_7+2n_8=106$. We define the disintegration KE as

$$\text{DKE} = \text{KE of initial cluster} - \text{KE of the fragments}. \tag{22}$$

In Fig. 7 we show $\text{DKE}^{\text{exact}}-\text{DKE}^{\text{approx}}$ for 273 processes described by Eq. (21), for several KE functionals. We see that our functional $T_s^{A0.185}$ is very accurate, improving over T_s^{TF} for all the configurations. $T_s^{A(1/6)}$ is close to, but better than the fourth-order gradient expansion T_s^{GE4}. Overall, this figure agrees well with the atomization KE of molecules reported in Table III, showing an important link between jellium spheres and molecules. These results and the liquid drop model [see Eq. (17) of Ref. 45] suggest that the TF functional gives a good balance between jellium surface KE and jellium curvature KE. This balance, which is important in atomization and disintegration processes, is improved by the *A*0.185-GGA functional.

IV. CONCLUSIONS

In this paper we have studied several semilocal KE density functionals derived from the Airy gas. These functionals, which depend trivially on the Laplacian of the density, do not satisfy several important constraints. Their kinetic energy densities are not always positive, and they implicitly violate the important constraint $\tau^{\text{approx}} \geq \tau^W$ (here τ^W is the von Weizsäcker KE density) and diverge to $-\infty$ at the nucleus of an atom.

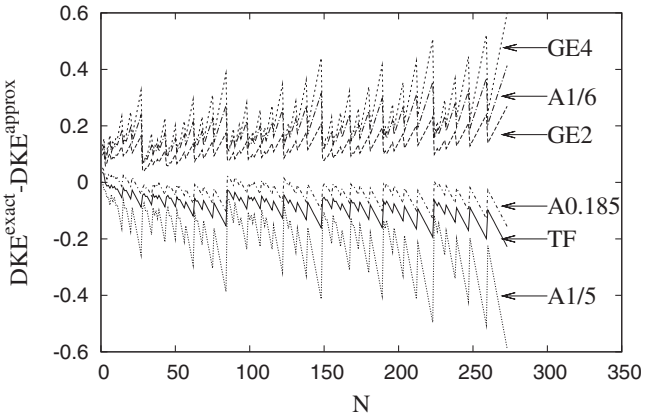

FIG. 7. Error of disintegration KE ($\text{DKE}^{\text{exact}}-\text{DKE}^{\text{approx}}$) for 273 configurations described by Eq. (21). The first point $N=1$ corresponds to $(106e^-)\rightarrow(92e^-)+(8e^-)+3\times(2e^-)$, and the last point $N=273$ corresponds to $(106e^-)\rightarrow 53\times(2e^-)$. We use OPM-KS orbitals and densities. Mean absolute errors are: $\text{m.a.e}^{\text{GE4}}=0.247$, $\text{m.a.e}^{A(1/5)}=0.218$, $\text{m.a.e}^{\text{GE2}}=0.128$, $\text{m.a.e}^{\text{TF}}=0.092$, $\text{m.a.e}^{A0.185}=0.039$, and $\text{m.a.e}^{A(1/6)}=0.196$. VJKS GGA, not shown in the figure, has $\text{m.a.e}^{\text{VJKS}}=0.165$.

However, such functionals can be accurate for the integrated KE of jellium surfaces and jellium clusters (e.g., $T_s^{A(1/6)}$), and of atoms and molecules (e.g., $T_s^{A0.185}$), when we use realistic densities (from KS calculations). More importantly, they are the most accurate KE density functionals, to our knowledge, for the integrated atomization kinetic energies of molecules and for the fragmentation of jellium clusters. These functionals may also be useful for quasirealistic densities (e.g., a superposition of free-atom Kohn-Sham densities), but they are not accurate enough for orbital-free calculations.

We have also presented a spin-unrestricted Hartree-Fock calculation for the stretched N_2 molecule that explains the N_2 atomization kinetic energies displayed in Table III, and that shows equilibrium lengths for many semilocal functionals. Thus, this work suggests that the spin-symmetry breaking and the spin scaling relations can be important tools in orbital-free approaches.

ACKNOWLEDGMENTS

We thank John P. Perdew for many valuable discussions and suggestions. L.A.C. acknowledges NSF support (Grant No. DMR05-01588).

[1] W. Kohn and L. J. Sham, Phys. Rev. **140**, A1133 (1965).

[2] An orbital-free kinetic energy density functional can be used in solving the spin-dependent Euler equations, or perhaps applied to a superposition of atomic Kohn-Sham or Hartree-Fock densities.

[3] V. V. Karasiev, R. S. Jones, S. B. Trickey, and F. E. Harris, in *New Developments in Quantum Chemistry*, edited by J. P. Paz and A. J. Hernández (Research Signpost, Kerala, 2009).

[4] W. Kohn and A. E. Mattsson, Phys. Rev. Lett. **81**, 3487 (1998).

[5] V. Sahni, C. Q. Ma, and J. S. Flamholz, Phys. Rev. B **18**, 3931

(1978).
[6] A. Solomatin and V. Sahni, Phys. Rev. B **56**, 3655 (1997).
[7] R. Baltin, Z. Naturforsch. A **27A**, 1176 (1972).
[8] D. A. Kirzhnitz, Sov. Phys. JETP **5**, 64 (1957); D. A. Kirzhnitz, *Field Theoretical Methods in Many-Body Systems* (Pergamon, Oxford, 1967)
[9] M. Brack, B. K. Jennings, and Y. H. Chu, Phys. Lett. **65B**, 1 (1976).
[10] R. M. Dreizler and E. K. U. Gross, *Density Functional Theory* (Springer-Verlag, Berlin, 1990).
[11] S. K. Ghosh and L. C. Balbas, J. Chem. Phys. **83**, 5778 (1985).
[12] L. Vitos, B. Johansson, J. Kollár, and H. L. Skriver, Phys. Rev. A **61**, 052511 (2000).
[13] J. P. Perdew and L. A. Constantin, Phys. Rev. B **75**, 155109 (2007).
[14] L. H. Thomas, Proc. Cambridge Philos. Soc. **23**, 542 (1927); E. Fermi, Rend. Accad. Naz. Lizei **6**, 602 (1927).
[15] N. D. Lang and W. Kohn, Phys. Rev. B **1**, 4555 (1970).
[16] E. Krotscheck and W. Kohn, Phys. Rev. Lett. **57**, 862 (1986).
[17] P. H. Acioli and D. M. Ceperley, Phys. Rev. B **54**, 17199 (1996).
[18] B. Wood, N. D. M. Hine, W. M. C. Foulkes, and P. García-González, Phys. Rev. B **76**, 035403 (2007).
[19] J. M. Pitarke and A. G. Eguiluz, Phys. Rev. B **63**, 045116 (2001).
[20] J. M. Pitarke, L. A. Constantin, and J. P. Perdew, Phys. Rev. B **74**, 045121 (2006).
[21] J. M. Pitarke and J. P. Perdew, Phys. Rev. B **67**, 045101 (2003).
[22] L. A. Constantin, J. M. Pitarke, J. F. Dobson, A. Garcia-Lekue, and J. P. Perdew, Phys. Rev. Lett. **100**, 036401 (2008).
[23] L. A. Constantin, J. P. Perdew, and J. Tao, Phys. Rev. B **73**, 205104 (2006).
[24] L. Vitos, B. Johansson, J. Kollár, and H. L. Skriver, Phys. Rev. B **62**, 10046 (2000).
[25] R. Armiento and A. E. Mattsson, Phys. Rev. B **72**, 085108 (2005).
[26] J. P. Perdew, A. Ruzsinszky, G. I. Csonka, O. A. Vydrov, G. E. Scuseria, L. A. Constantin, X. Zhou, and K. Burke, Phys. Rev. Lett. **100**, 136406 (2008); **102**, 039902(E) (2009).
[27] J. P. Perdew, L. A. Constantin, E. Sagvolden, and K. Burke, Phys. Rev. Lett. **97**, 223002 (2006).
[28] C. F. v. Weizsäcker, Z. Phys. **96**, 431 (1935).
[29] In the tail of a spherical atom, the density decays exponentially as $n(\mathbf{r})=\gamma e^{-\alpha r}$, so $s^2\to\infty$ when $r\to\infty$, and $\nabla^2 n\to(40/3)\tau^{\mathrm{TF}}s^2$ in this asymptotic region.
[30] D. García-Aldea and J. E. Alvarellos, J. Chem. Phys. **129**, 074103 (2008).
[31] R. Monnier and J. P. Perdew, Phys. Rev. B **17**, 2595 (1978).
[32] G. L. Oliver and J. P. Perdew, Phys. Rev. A **20**, 397 (1979).
[33] E. Clementi and C. Roetti, At. Data Nucl. Data Tables **14**, 177 (1974).
[34] S. Kümmel and John P. Perdew, Phys. Rev. Lett. **90**, 043004 (2003) and references therein.
[35] S. S. Iyengar, M. Ernzerhof, S. N. Maximoff, and G. E. Scuseria, Phys. Rev. A **63**, 052508 (2001).
[36] A. D. Becke, Phys. Rev. A **38**, 3098 (1988).
[37] J. P. Perdew, in *Electronic Structure of Solids '91*, edited by P. Ziesche and H. Eschrig (Akademie Verlag, Berlin, 1991).
[38] F. Tran and T. A. Wesolowski, Int. J. Quantum Chem. **89**, 441 (2002).
[39] M. Fuchs, Y.-M. Niquet, X. Gonze, and K. Burke, J. Chem. Phys. **122**, 094116 (2005) and references therein.
[40] A. M. Lee and N. C. Handy, J. Chem. Soc., Faraday Trans. **89**, 3999 (1993).
[41] O. Gunnarsson and B. I. Lundqvist, Phys. Rev. B **13**, 4274 (1976).
[42] J. P. Perdew, A. Savin, and K. Burke, Phys. Rev. A **51**, 4531 (1995).
[43] J. A. Pople, P. M. W. Gill, and N. C. Handy, Int. J. Quantum Chem. **56**, 303 (1995).
[44] B.-G. Englert, *Semiclassical Theory of Atoms (Lecture Notes in Physics)* (Springer-Verlag, Berlin, 1988) (and references therein).
[45] D. Lee, K. Burke, L. A. Constantin, and J. P. Perdew, J. Chem. Phys. **130**, 034107 (2009).